Available online at www.sciencedirect.com
SCIENCE DIRECT®
Journal of Non-Crystalline Solids 351 (2005) 1949–1957
JOURNAL OF NON-CRYSTALLINE SOLIDS
www.elsevier.com/locate/jnoncrysol

Synthesis and spectroscopic study of mixed metal clusters using methacrylate and acrylate ligands

J. Méndez-Vivar [a,*], P. Bosch [b], V.H. Lara [a]

[a] Universidad Autónoma Metropolitana-Iztapalapa, Depto. de Química, AP 55-534, México DF 09340, México
[b] Instituto de Investigaciones en Materiales, UNAM, Circuito Exterior, Ciudad Universitaria, México DF 04510, México

Received 7 July 2004; received in revised form 12 May 2005
Available online 20 June 2005

Abstract

Methacrylate and acrylate ligands derived from 3-(trimethoxysilyl) propil methacrylate (TMSPM), 2-hydroxy ethyl methacrylate (HEM) and acrylic acid (AA) were used to obtain clusters of Ti and Zr from a sol–gel polymerization. The spectroscopic techniques used for the characterization included small angle X-ray scattering (SAXS), Fourier transform infrared spectroscopy (FTIR), UV–Vis spectroscopy and X-ray diffraction (XRD). The acrylate ion acted as a chelating agent, whereas methacrylates derived from HEM and TMSPM acted as bridging agents, according to the results. The experimental strategy can be used to tailor the structure of amorphous solids.

1. Introduction

Modifying agents that can act as a mono or bidentate ligands are used in sol–gel processing of metal alkoxides to control their reactivity, due to a decreasing of the chemical functionality and a simultaneous increase of the metal coordination number [1–3]. In this way, the chemical reactivity of pure alkoxides is slowed-down, allowing to tailor the polymer structure. Typical examples of such compounds are the carboxylates, ß-diketonates and sulfonates [4,5]. Methacrylate or acrylate-containing molecules such as 3-(trimethoxysilyl) propyl methacrylate (TMSPM), 2-hydroxy ethyl methacrylate (HEM) and acrylic acid (AA), are particularly interesting as ligands in the polycondensation of Ti–Zr sols, as they can form new precursors for hybrid organic–inorganic polymers [6,7].

The purpose of combining Ti and Zr clusters is to improve the chemical properties of the products derived from these polymers, (i.e. films, ceramics, fibers, etc.) compared to those that contain only one of these ions. In this way, Zr as ZrO_2 provides chemical stability in harsh environments and Ti as TiO_2 provides thermal stability, avoiding phase changes of the solid product [1,2,5,26].

The goal of this research was to synthesize and study by spectroscopic techniques Ti–Zr oligomeric structures via modification of the alkoxide precursors using molecules containing methacrylates or acrylates as stabilizing agents. The study was done by spectroscopic techniques (FTIR, UV–Vis) and SAXS mainly.

2. Experimental

2.1. Clusters prepared using 3-(trimethoxysilyl) propyl methacrylate (TMSPM)

5.53×10^{-3} mol of titanium isopropoxide ($Ti(OPr^i)_4$) (Aldrich, 97.0%) were mixed by continuous stirring with 5.53×10^{-3} mol of zirconium *n*-propoxide ($Zr(OPr^n)_4$) (Aldrich, 70.0%) at room temperature (298 K).

* Corresponding author. Tel.: +5258 04 46 64; fax: +5258 04 46 66.
E-mail address: jmv@xanum.uam.mx (J. Méndez-Vivar).

0022-3093/$ - see front matter © 2005 Elsevier B.V. All rights reserved.
doi:10.1016/j.jnoncrysol.2005.05.014

49.77×10^{-3} mol of TMSPM (Aldrich, 97.0%) were added at room temperature while stirring. The reactions were performed in an open vessel, allowing that H_2O from environmental moisture hydrolized the alkoxides. The molar ratios Ti:Zr:TMSPM were 1.0:1.0:9.0, respectively. Additional sols with the molar ratios 1.0:2.0:9.0 and 1.0:2.0:18.0 were also prepared. The sols were left stirring overnight and then storaged in a dessicator for later analysis.

The same procedure was followed to obtain Ti–Zr clusters using separately 2-hydroxy ethyl methacrylate (HEM, Aldrich, 97.0%) and acrylic acid (AA, Aldrich, 99.0%) as modifying agents. In the latter case an additional amount of H_2O was produced for the hydrolisis step, as a result of the esterification reaction between AA and *n*PrOH, the solvent; see Scheme 1. The fresh sols were studied by FTIR and SAXS. After gellation or phase separation, the samples were dried at 423 K in air. The xerogels were studied by XRD.

2.2. Characterization techniques

A Perkin–Elmer λ40 spectrophotometer was used to obtain the UV–Vis spectra in the 200–800 nm region. Quartz cells were used and isopropanol (Sigma, 99.0%) was the solvent. FTIR spectra of the sols were obtained using a Perkin–Elmer 1600 spectrophotometer in the 4000–400 cm^{-1} region using nujol as the solvent. The samples were deposited between KBr plates and then analyzed. The FTIR study of the solids was done using KBr pellets.

The small angle X-ray scattering (SAXS) measurements of the sols were done with an equipment composed of a Kratky camera coupled to a copper anode tube. A Nickel filter selected the Kα radiation. The collimated X-ray beam was linear and corresponded to an 'infinitely high' beam. The sol samples were introduced in a capillary tube. The SAXS data collected with a proportional linear counter were processed as suggested by Glatter (ITP program) [8,9], where the angular parameter h, in reciprocal angstroms, is defined as $h = (4\pi/\lambda)\sin(\theta/2)$, where θ and λ are the scattering angle and the wavelength of the X-ray, respectively.

The radius of gyration of the sols were obtained from the slope of the curve $\log I(h)$ versus h^2 of the Guinier plot [10]. In SAXS experiments, the $\log I(h)$ versus $\log h$ plot provides the fractal dimension [11], which is an useful parameter to differentiate the degree of aggregation of the internal structure of the scattering object. The h interval to obtain the fractal dimensions was $0.07 < h < 0.18$ $Å^{-1}$.

The shape of the oligomers in the sols was estimated from the Kratky plot, $h^2I(h)$ versus h. If the Kratky curve presents a broad peak, the scattering particles, most probably, present a globular conformation, whereas if the curve approximates to a plateau, the particles, most probably, have a fiber-like shape [12]. If the shape is known, it is possible to calculate the distance distribution functions [13]. These distributions provide a criterion to estimate the polydispersity.

A Siemens D500 diffractometer coupled to a copper X-ray diffraction tube was used to obtain conventional X-ray diffraction patterns of the xerogels. Again, a Siemens D500 diffractometer, but coupled to a molybdenum X-ray diffraction tube was used to ensure to reach the high values of the h parameter ($h = 4\pi\sin\theta/\lambda$) required to obtain the radial distribution functions. The Kα radiation was selected with a filter, and the data measured by step scanning with a scintillation counter, were the input of the Radiale program [14].

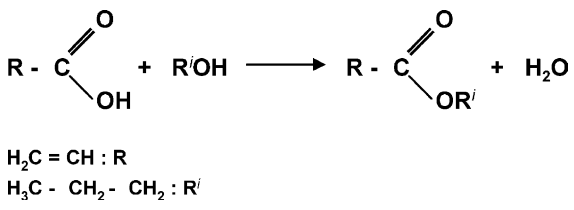

Scheme 1. Esterification reaction.

3. Results

The stability of the sols was variable, as it can be seen in Table 1. The Ti–Zr–TMSPM sols were those with the shortest gellation times, in about 24 h at room temperature, giving as a result white gels. On the other hand, the Ti–Zr–HEM sols gelled around 48 h producing clear yellow gels, whereas phase separation occurred for the Ti–Zr–AA sols after about 4 months. In the latter case both, the sols and precipitates were amber color.

3.1. FTIR

The FTIR results of the Ti–Zr–CA (CA: chelating agent) sols aged 1 week at room temperature are presented in Tables 3–5. In the cases where HEM and TMSPM were used, the corresponding gels were actually analyzed, as the gelation times for these samples were 48 h and 24 h, respectively; see Figs. 6–8.

3.2. UV–Vis

The results for fresh Ti–Zr–AA sols appear in Table 6 and in Fig. 9. In addition, the spectra of Ti–Zr–HEM sols were also obtained. In all cases a single band at 211–213 nm was obtained, accompanied by a shoulder at 250 nm. We propose that these bands can be assigned to Zr ← O and to Ti ← O charge transference bands, respectively. Regarding the Ti–Zr–TMSPM sols, it was not possible to obtain accurate spectra due to the very short gelation times (24 h).

Table 1
Physical appearance of sols and gels

Sample	Molar ratio Ti:Zr:CA	Color	Remarks
Ti–Zr–AA	1.0:1.0:9.0	Amber sol	Phase separation after 4 months at room temperature (293 K)
	1.0:2.0:9.0	Amber sol	Phase separation after 4 months at room temperature
	1.0:2.0:18.0	Amber sol and white precipitate as sediment	Phase separation occurs after 5 weeks at room temperature
Ti–Zr–HEM	1.0:1.0:9.0	Yellow	Gelation time: 48 h sineresis
	1.0:2.0:9.0	Yellow	Gelation time: 48 h sineresis
	1.0:2.0:18.0	Opaque yellow	Gelation time: 48 h sineresis
Ti–Zr–TMSPM	1.0:1.0:9.0	White	Gelation time: 24 h
	1.0:2.0:9.0	White	Gelation time: 24 h
	1.0:2.0:18.0	White	Gelation time: 24 h

Table 2
SAXS results of fresh Ti–Zr–CA (CA: chelating agent) sols with the molar ratios 1.0:1.0:9.0

Sol	Fractal dimension (D_f)	Radius or gyration (Å)	Structure
Ti–Zr–AA	2.0	183	Linear
Ti–Zr–HEM	1.8	114	Multiparticle diffusion-limited aggregate
Ti–Zr–TMSPM	1.8	143	Multiparticle difussion-limited aggregate

Table 3
FTIR results of Ti–Zr–AA sols aged 1 week at room temperature

Assignment	Wavenumber (cm^{-1}) Ti:Zr:AA molar ratio		
	1.0:1.0:9.0	1.0:2.0:9.0	1.0:2.0:18.0
O–H stretching [15]	3345 w	3346 m	3400 w
C–H stretching [16]	2965 SH, s	2923 SH, s	2930 SH, s
C=O stretching [15]	1718 m	1731 SH, s	1728 SH, s
C=C stretching [17]	1636 w, SH	1637 m, SH	1637 m, SH
O–C=O from AA bonded to Ti and to Zr as an asymmetric chelate. This work	1538 W, w	1538 m	1541 m
CH_2, CH_3 bending [15]	1449 m	1456 m	1456 s
C–O–Ti stretching [18]	1376 SH, m	1375 SH, m	1376 SH, s
C–O–Zr stretching [18]	1296 w	1272 m	1273 m
C–O stretching [15]	1180 w	1190 m	1191 m
	1066 m	1066 m	1066 s
O–C–O–Ti as a bridge [19]	967 w	967 m	984 s
CH_2 and CH_3 [15]	828 w	829 m	828 m
Ti–O–Ti [20]	680 w	700 w	695 w
		660 w	650 w
Zr–O [21]	625 w		

w: Weak, m: medium, SH: sharp, s: strong, W: wide.

3.3. X-ray diffraction

Fig. 2 shows the results obtained for Ti–Zr–AA xerogels with different molar composition: 1.0:1.0:9.0 (Fig. 2(a)); 1.0:2.0:9.0 (Fig. 2(b)), 1.0:2.0:18.0 (Fig. 2(c)), and the amber sol with the molar composition 1.0:2.0:18.0 (Fig. 2(d)). Fig. 2(a) and (b) are similar. Both samples present a single sharp and well defined peak at $2\theta = 5.5°$ (interplanar distance of 16 Å showing that a recurrent order is present). The diffractograms correspond to a non-crystalline compound as no other clear peaks are observed. The sample with the molar composition 1.0:2.0:18.0 was constituted by a precipitate and a liquid phase. Comparing Fig. 2(c) and (d), it can be noted that a weak peak appears at $d = 16$ Å in Fig. 2(c); on the other hand, no signal at all was present in the sol. We also studied by XRD the calcined samples in air at 873 and 1173 K (results not shown here). All the solids were amorphous in those conditions.

Table 4
FTIR results of Ti–Zr–HEM gels aged 1 week at room temperature

Assignment	Wavenumber (cm^{-1}) Ti:Zr:HEM molar ratio		
	1.0:1.0:9.0	1.0:2.0:9.0	1.0:2.0:18.0
O–H stretching [15]	3200 W, w	3497 m	3441 m, W
C–H stretching [16]	2929 m	2929 s	2958 m
C=O stretching [15]	1714 s	1713 vs, SH	1722 vs, SH
C=C stretching [17]	1634 m	1638 s, SH	1638 m
O–C=O from HEM bonded to Ti and to Zr. This work	1556 m	1555 m	1550 w
CH_2, CH_3 bending [15]	1454 m	1454 s	1455 m
Symmetric and asymmetric C–H [15]	1400 w	1405 w	1404 w
C–O–Ti stretching [18]	1370 w	1378 w	1390 w
C–O–Zr stretching [18]	1320 s	1320 s	1321 s
	1297 s	1297 s	1305 s
C–O stretching [15]	1168 s	1167 s	1168 vs
	1084 s	1083 s	1083 m
O–C–O–Ti as a bridge [19]	950 w	941 w	944 m
Ti–O [15]	815 SH, m	815 SH, vs	816 SH, m
Ti–O–Ti [20]		650 sh	650 w
Zr–O [21]	616 s, W	613 s, W	614 m

w: Weak, m: medium, SH: sharp, s: strong, W: wide, vs: very strong, sh: shoulder.

3.4. Radial distribution functions

The radial distribution functions (RDF) appear in Fig. 3: TiO_2 as reference (Fig. 3(a)), ZrO_2 as reference

Table 5
FTIR results of Ti–Zr–TMSPM gels aged 1 week at room temperature

Assignment	Wavenumber (cm^{-1}) Ti:Zr:TMSPM molar ratio		
	1.0:1.0:9.0	1.0:2.0:9.0	1.0:2.0:18.0
C–H stretching [16]	2961 s	2960 m	2961 s
C=O stretching [15]	1714 SH, vs	1717 SH, s	1722 SH, vs
O=C–O–R in methacrylate	1634 SH, m	1636 SH, m	1639 SH, m
C=C in methacrylate	1574 w	1574 w	1550 w
CH_2, CH_3 bending [15]	1454 m	1457 m	1454 m
C–O–Ti stretching [18]	1402 m	1376 m	1376 m
C–O–Zr stretching [18]	1297 s	1297 m	1297 s
Si–O–CH_3 rocking [15]	1168 s	1165 m	1167 s
O=C–O–C [15]	1088 s, W	1086 m, W	1087 s, W
Si–O–Ti	950 w	970 w	950 w
Si–O–Zr [22]	750 w	745 w	740 w
Ti–O–Ti [22]	655 w, SH	668 m, SH	650 w
Si–O–Si [23]	418 s, W	462 m, W	462 m, W

w: Weak, m: medium, SH: sharp, s: strong, W: wide, vs: very strong.

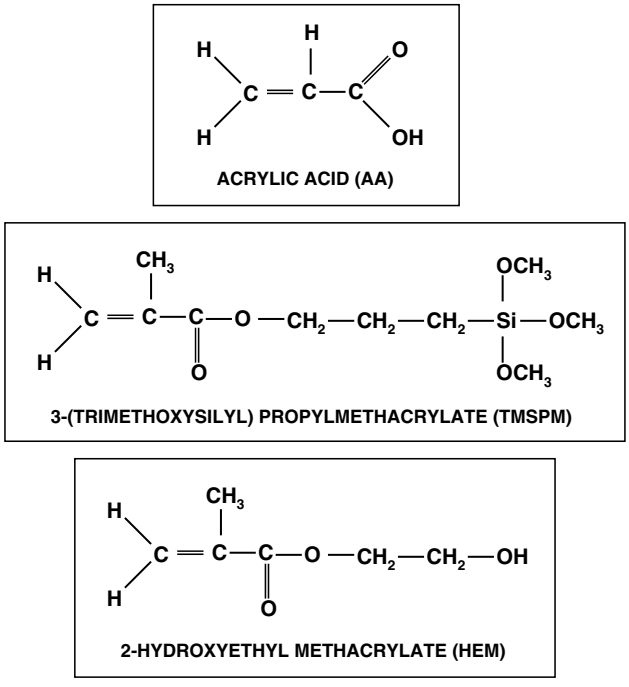

Fig. 1. (a) AA, (b) HEM and, (c) TMSPM molecules.

(Fig. 3(b)), and Ti–Zr–AA xerogels; 1.0:1.0:9.0 (Fig. 3(c)); 1.0:2.0:9.0 (Fig. 3(d)), 1.0:2.0:18.0 (Fig. 3(e)), and the amber sol with the molar composition 1.0:2.0:18 (Fig. 3(f)). The peaks corresponding to the most probable interatomic distances fade out for a radial distance of 5 Å in the three solid samples. Therefore, the obtained materials are constituted by small crystalline particles whose size is smaller than 10 Å in diameter embedded in an amorphous phase. The liquid

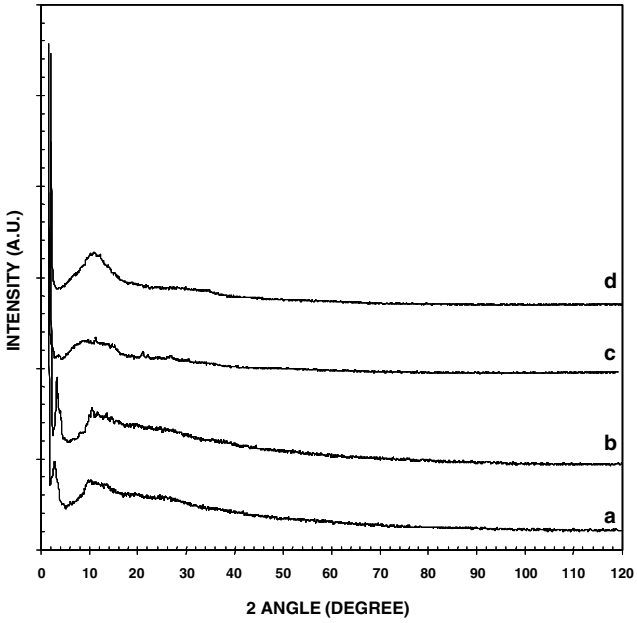

Fig. 2. X-ray diffraction results of Ti–Zr–AA xerogels: (a) 1.0:1.0:9.0, (b) 1.0:2.0:9.0, (c) 1.0:2.0:18.0 and, (d) the sol with the molar composition 1.0:2.0:18.0.

fraction of the 1.0:2.0:18.0 sample (Fig. 3(f)) seems to be more structured and will also be discussed.

3.5. SAXS

The Ti–Zr–CA (CA: chelating agent) sols were studied at room temperature in the Guinier region to determine the fractal dimension (D_f) and radius of gyration (R_g) values, same as the oligomer structure. The results appear in Table 2. The oligomer structures were determined by the corresponding Kratky plots.

The shape of the heterogeneities (structured particles or agglomerates) present in the samples was estimated from the Kratky plots (Fig. 4). Assuming those shapes, the corresponding particle size distributions were calculated; see Fig. 5. As the Kratky plots of the samples HEM (Fig. 4(b)) and TMSPM (Fig. 4(c)) present a peak, the shape should be globular whereas in the case of AA (Fig. 4(a)) the scattering objects must be fibrillar.

4. Discussion

The molecules AA, HEM and TMSPM are presented in Fig. 1 in order to clarify the discussion. The three stabilizing agents AA, HEM and TMSPM exhibited different results when they reacted with Ti and Zr. One of the most important differences is that the acrylic acid (AA) also acted as a catalyst during the hydrolysis step of the Ti and Zr alkoxides. In this way, the esterification reaction between AA and *n*-propanol, the solvent alcohol

accompanying the alkoxides occurred to some extent, producing H_2O, accelerating the hydrolysis of Ti and Zr alkoxides; see Scheme 1. However, gellation did not occur in any of the Ti–Zr–AA sols, because simultaneously the acrylate ion derived from AA acted as a chelating agent, leading to a gradual, controlled hydrolysis; see Scheme 2. Precipitation of a white powder in a short time (5 weeks) was only observed in the case of the sol with the highest content of AA, corresponding to the molar ratios 1.0:2.0:18.0 (Ti–Zr–AA, respectively). This result can be attributed to an excess of H_2O produced in this case, as a result of the esterification reaction.

The opacity of the Ti–Zr–TMSPM sols and the short gellation time (24 h) can be attributed to the preferential reactions between the hydrolyzed Ti and Zr species (quickly produced in presence of the atmospheric moisture) and the siloxane groups, compared to the bonding of Ti and Zr to the pendant oxygen of the methacrylate group; see Schemes 3–5. In this way, stabilization of Ti and Zr via chelation was not accomplished using TMSPM.

All the sols prepared with HEM polymerized in 48 h giving as a result yellow gels. The most marked feature of these gels compared to the products obtained in the other cases was the syneresis. In this case the elimination of the solvent form the gel pores once the gel was formed was due to condensation reactions that still were taking place. The syneresis can be attributed directly to the OH functional group of HEM. In this way, some of those unreacted OH groups bonded to hydrolyzed but not condensed Ti or Zr species after gellation produced H_2O; see Scheme 6.

According to the FTIR results, the bonding of the $^{-}OC{=}O$ group to Ti and to Zr appeared in the ranges

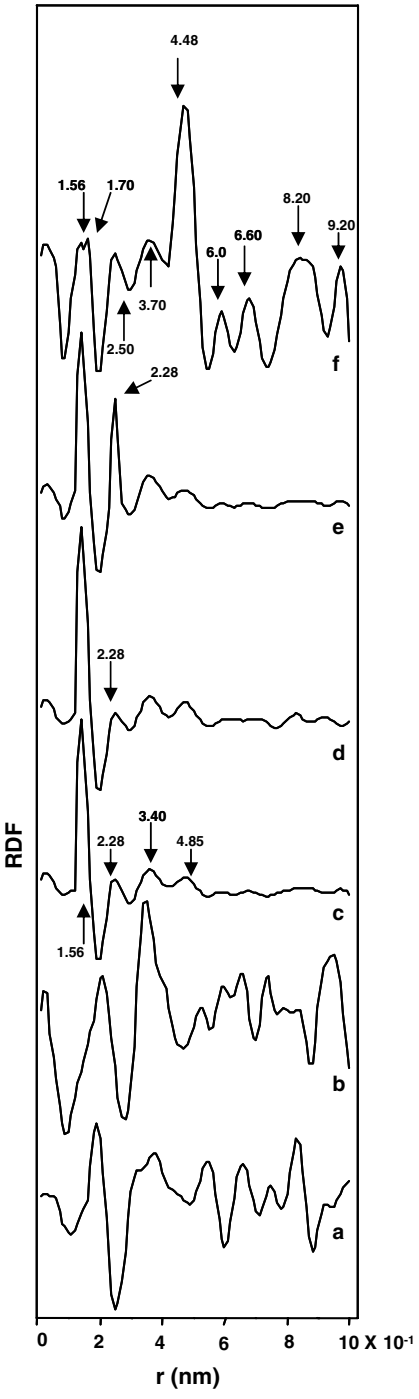

Fig. 3. Radial distribution functions (RDF) of: TiO_2 as reference (a), ZrO_2 as reference (b), and Ti–Zr–AA xerogels; 1.0:1.0:9.0 (c); 1.0:2.0:9.0 (d); 1.0:2.0:18.0 (e) and, the sol with the molar composition 1.0:2.0:18.0 (f).

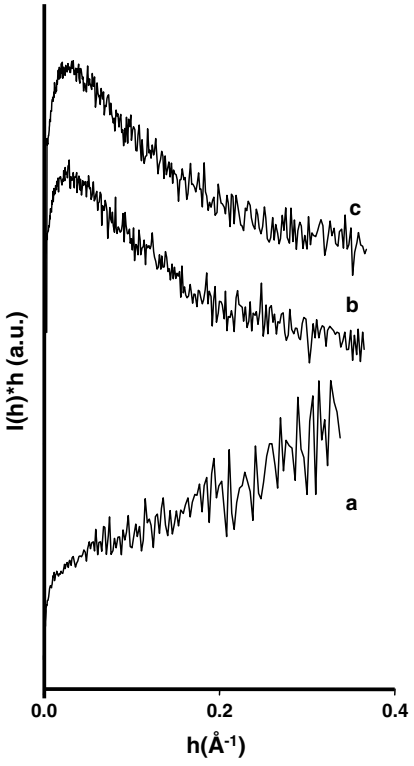

Fig. 4. Kratky plots of the xerogels: (a) Ti–Zr–AA (1.0:2.0:9.0), (b) Ti–Zr–HEM (1.0:1.0:9.0) and, (c) Ti–Zr–TMSPM (1.0:1.0:9.0).

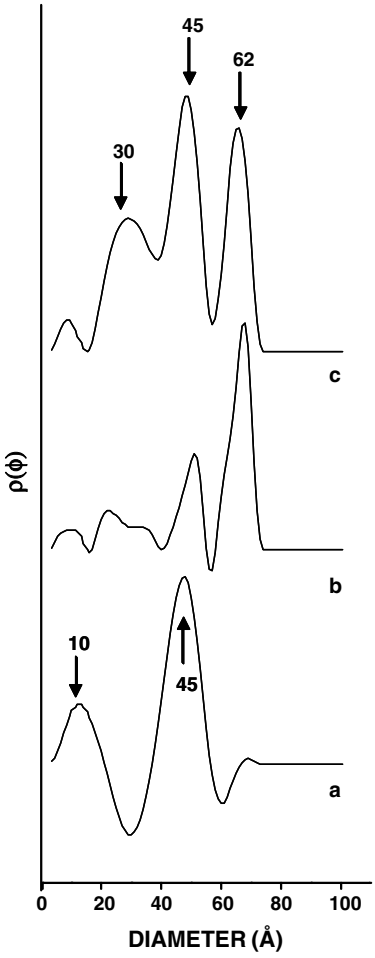

Fig. 5. Particle size distribution of the xerogels: (a) Ti–Zr–AA (1.0:2.0:9.0), (b) Ti–Zr–HEM (1.0:1.0:9.0) and, (c) Ti–Zr–TMSPM (1.0:1.0:9.0).

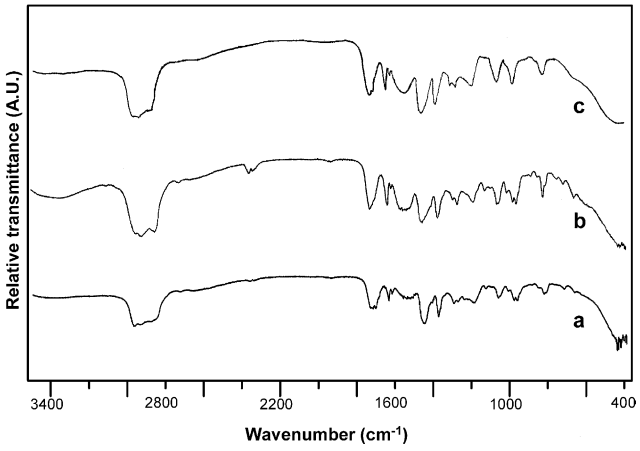

Fig. 6. FTIR spectra of Ti–Zr–AA sols aged 1 week at room temperature: (a) 1.0:1.0:9.0, (b) 1.0:2.0:9.0, (c) 1.0:2.0:18.0.

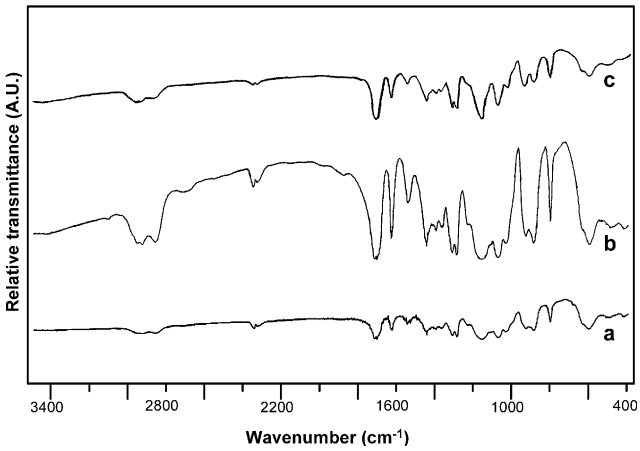

Fig. 7. FTIR spectra of Ti–Zr–HEM gels aged 1 week at room temperature: (a) 1.0:1.0:9.0, (b) 1.0:2.0:9.0, (c) 1.0:2.0:18.0.

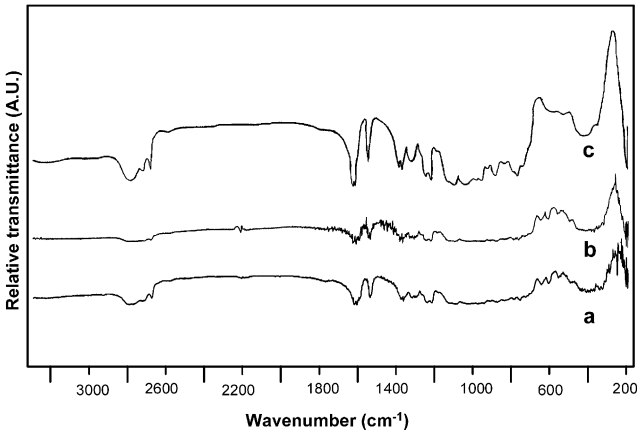

Fig. 8. FTIR spectra of Ti–Zr–TMSPM gels aged 1 week at room temperature: (a) 1.0:1.0:9.0, (b) 1.0:2.0:9.0, (c) 1.0:2.0:18.0.

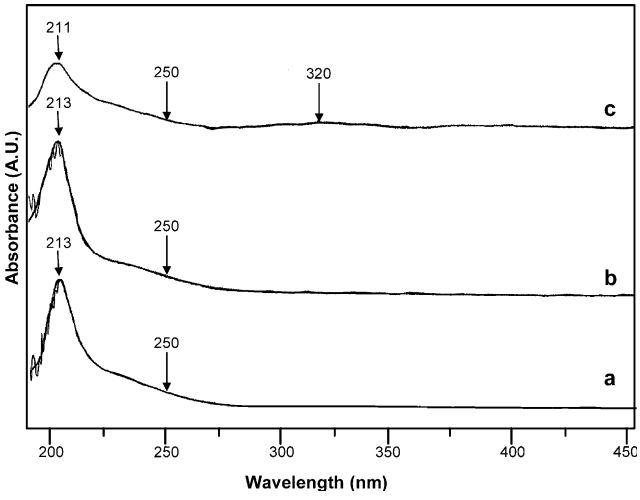

Fig. 9. UV–Vis spectra of fresh Ti–Zr–AA sols: (a) 1.0:1.0:9.0, (b) 1.0:2.0:9.0, (c) 1.0:2.0:18.0.

1538–1541 cm^{-1}, 1550–1556 cm^{-1}, and 1550–1574 cm^{-1} for the sols containing AA, HEM and TMSPM, respectively (see Tables 3–5). The sols that gelled first were those containing TMSPM (24 h), then those containg HEM (48 h) and finally, phase separation occurred for the ones containing AA (from 5 weeks, up to 4 months).

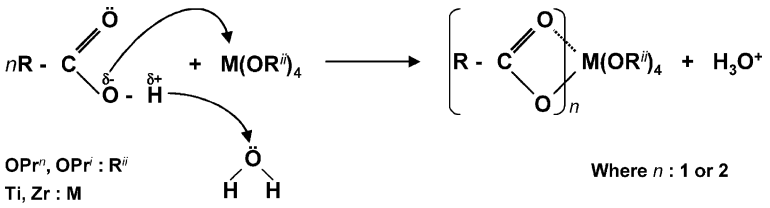

Scheme 2. Metal alkoxides chelation.

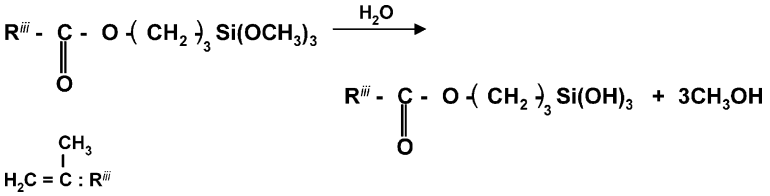

Scheme 3. TMSPM hydrolysis reaction.

Scheme 4. Metal alkoxides hydrolysis.

Then, the wavenumber shiftings are consistent with the gellation times, and can be used as indicators of the bonding strength between the stabilizing agents and the metal ions. Based on these findings, we suggest that the smaller acrylate ion resulting from AA predominantly formed chelates with Ti and Zr, whereas the larger HEM and TMSPM ions mainly formed bridges between the metal ions. This reasoning is supported by the UV–Vis results, presented in Table 6, and in Fig. 9 where a weak band at 320 nm appeared in the sol with the molar composition 1.0:2.0:18.0. This band can be assigned to the acrylate ion bonded to Ti and to Zr as a bidentate ligand. Additional supporting results of this reasoning was found in the SAXS results shown in Table 2. The fractal dimension value obtained for the sol containing AA (2.0) corresponds to a linear structure as a result of a controlled hydrolysis–condensation process, whereas the value for the sols containing HEM and TMSPM (1.8), corresponds to multiparticle diffusion-limited aggregates, resulting from the condensation of species where the modifying agents were bonded to Ti and Zr as monodentate ligands only.

We identified the C–O–Zr bonds at lower wavenumbers in all cases (1272–1321 cm^{-1}) compared to the C–O–Ti bonds (1370–1402 cm^{-1}). In addition, the Ti–O–Ti bonds were detected in all cases, indicating the formation of Ti oligomers. The O–C–O–Ti bonds as bridges were detected in all cases in the region 941–984 cm^{-1}. We do not have any indication that this type of bonds were formed with Zr. In the case of the sols containing TMSPM, the Si–O–Ti and Si–O–Zr bonds were detected at 815–820 cm^{-1} and 740–750 cm^{-1},

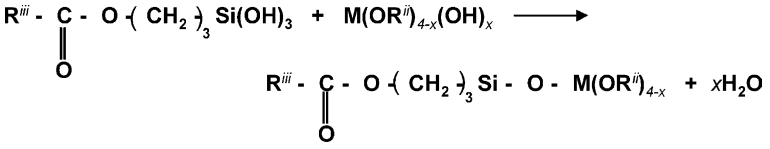

Scheme 5. Reaction between hydrolized TMSPM and partially hydrolized metal alkoxides.

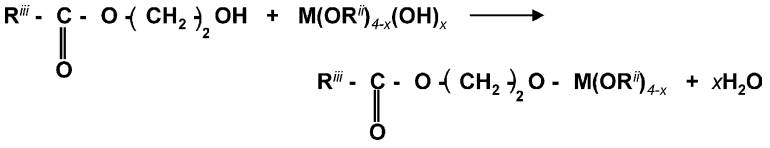

Scheme 6. Reaction between HEM and partially hydrolized metal alkoxides.

Table 6
UV–Vis results of fresh Ti–Zr–AA sols

Assignment	Wavelength (nm)		
	1.0:1.0:9.0	1.0:2.0:9.0	1.0:2.0:18.0
Zr ← O This work	213	213	211
Ti ← O This work	250 sh	250 sh	250 sh
$\pi^* \leftarrow \pi$ Transition of acrylate ion bonded to Ti and to Zr as a bidentate ligand. This work	–	–	320 w

sh: Shoulder, w: weak.

respectively. Apparently the affinity between siloxanes and the alkoxy species of the metal ions Ti and Zr was stronger compared to the bonding between TMSPM and Ti or Zr, as these sols gelled in 24 h. In addition, the formation of Si–O–Si oligomers was also detected at 418–462 cm^{-1}.

Regarding the RDF, the structure of the small agglomerates (Fig. 3(c)–(e)) present a first neighbor interatomic distance of 0.156 nm (note that the length scale in Fig. 3 is multiplied by 10^{-1}). This distance could be attributed to C–O bonds (0.153 nm) from organic groups still present in the xerogels. The ionic distances of the Ti–O and Zr–O bonds are 0.196 and 0.219 nm, respectively. Hence, although it is not possible to assign the Ti–O distance, the peak at 0.228 nm in Fig. 3(c)–(e) can be attributed to Zr–O.

When the solid samples 1.0:2.0:9.0 (Fig. 3(d)) and 1.0:2.0:18.0 (Fig. 3(e)) are compared, a difference on the size of the peak at 0.228 nm can be observed. The difference can be correlated to the molar composition of AA which is twice in the latter case. Apparently, in this case ZrO_2 is formed as a result of the esterification reaction of AA with the solvent, leading to an uncontrolled hydrolysis of $Zr(OPr^n)_4$ and ultimately to a phase separation. However, amorphous ZrO_2 was only produced, as all the XRD patterns corresponded to amorphous solids.

In Fig. 3(c)–(e) peaks also appear at 0.34 and 0.485 nm. These values differ from those present in TiO_2 and ZrO_2. In rutile, for instance the cell parameters are 0.449 and 0.289 nm, which are distances between Ti–Ti or O–O. Metal atoms are the center of deformed octahedrons constituted by oxygens and in turn each oxygen is surrounded by three metal atoms in the same plane. Then, to explain our values, we can assume that the 0.34 nm distance is an O–O distance. We suggest that the peak found at 0.485 nm can be assigned to metal–metal relaxed distances in rutile structure [25]. Note that some of the obtained values in our radial distribution functions differ from those reported by Schubert et al. (i.e. in their case the distances between Zr and O are 0.217 and 0.228 nm, whereas the distances between Ti and O are 0.182 and 0.203 nm) [7]. The differences can be attributed to: (a) the molecular complexity of the precursors; in our case we employed monomeric alkoxides ($Ti(OPr^i)_4$ and $Zr(OPr^n)_4$), compared to the oligomeric precursors used by them ($Ti(OBu)_4$ and $Zr(OBu)_4$), (b) the chelating agent that in our case was acrylic acid (AA), compared to methacrylic acid in their case and, (c) the composition (molar ratios) of the sols. In addition, the role of the alkyl group size in an alkoxide in a sol–gel polymerization must be considered, because it exerts an influence on the morphology (particle size, surface area) and crystallization behavior of the resulting gel.

The shape of the radial distribution function corresponding to the liquid phase of sample Ti–Zr–AA (1.0:2.0:18.0) can be seen in Fig. 3(f). It is different from the other distributions (Fig. 3(c)–(e)). Order is present up to a radial distance of 1.0 nm and peaks are rather broad indicating that several atomic distances are similar. The first peak is resolved as two peaks; the first one at $r = 0.156$ nm (this distance was observed in the previously discussed samples) and 0.17 nm. These peaks could be attributed to Ti–O and C–O distances. The second peak at 0.25 nm may be due to some organic distance and the third one, at 0.37 nm corresponds to an O–O or metal–metal bond. This part of the distribution reproduces the structure of the clusters found in the solid samples, although an extra distance was found at 0.17 nm. The peak at 0.448 nm is very high and can be assigned to Ti–Ti or to O–O distances. The peaks at higher distances are due to second and third neighbors present in the liquid, which shows that the structure is fairly ordered even at high distances. Then, in this fraction of the sample the homogeneity is better than in the precipitated fraction, which is constituted by small clusters. Although the long range order in liquids is lower than in gels or xerogels, in these samples the opposite behavior is observed. This difference has to be understood as follows. In the xerogels well ordered domains up to a radius of 0.45 nm are formed, but in the liquid the order is more homogeneous and these locally ordered domains are not present. Hence, the xerogels are inhomogeneous whereas the liquid is homogeneous up to a distance of 1.0 nm.

According to the results presented in Table 2 the fractal dimension for the samples prepared with HEM and TMSPM is the same, 1.8. The corresponding value for the sample prepared with AA turns out to be 2.0, indicating that in this sol the structures are more compact and that the degree of connectivity between the particles is higher. These values may be compared to those reported by Schaefer and Keefer [24]. A mass fractal dimension of 2.0 is attributed to linear polymers whereas a value of 1.8 corresponds to multiparticle diffusion-limited aggregates.

The radius of gyration for the AA sample is the highest. The clusters then are more compact and definitely larger. The radius of gyration is a parameter depending

on the size but not on the shape of the clusters. Comparing the radius of gyration of the samples prepared with HEM and TMSPM, differences can be observed. As their fractal dimension is the same (1.8), their structure is equivalent as far as connectivity is concerned, but the size is larger in TMSPM. According to this result, TMSPM allowed the condensation of the oligomeric chains containing Ti and Zr to a larger extent compared to HEM producing larger clusters. The corresponding particle size distributions are very different. The sample TMSPM presents a peak at $r = 30$ Å (see Fig. 5(c)) which is not present in any of the other samples. This result also explain the shortest gellation time of the sols (24 h), due to the highest condensation rate, as it was discussed before. Otherwise, the agglomerates are quite similar in HEM and TMSPM (Fig. 5(b) and (c), respectively) and turn to be 45 and 62 Å radii. The linear agglomerates present in the AA sample have two characteristic radii: 10 and 45 Å.

5. Conclusion

The molecular complexity and the functional groups of the modifying agents allowed to obtain different clusters, characterized by SAXS. The acrylate ion acted mainly as a chelating agent in the clusters formation, whereas methacrylates derived from HEM and TMSPM acted as bridging agents, according to the FTIR, UV–Vis and SAXS results. The developed experimental strategy can be used to tailor amorphous solids. In all cases the sols can be used as precursors for hybrid organic–inorganic polymers in subsequent studies.

References

[1] C.J. Brinker, G.W. Scherer, Sol–gel Science, the Physics and Chemistry of Sol–gel Processing, Academic, San Diego, CA, 1990.
[2] J.D. Mackenzie, D.R. Ulrich (Eds.), Ultrastructure Processing of Advanced Ceramics, Wiley, New York, 1988.
[3] C. Sanchez, M. In, J. Non-Cryst. Solids 147&148 (1992) 1.
[4] A. Léaustic, F. Babonneau, J. Livage, Chem. Mater. 1 (1989) 248.
[5] J. Méndez-Vivar, R. Mendoza-serna, L. Valdez-Castro, J. Non-Cryst. Solids 288 (2001) 200.
[6] G. Kickelbick, U. Schubert, Organic/inorganic hybrid materials, in: R.M. Laine, C. Sanchez, C.J. Brinker, E. Giannelis (Eds.), Materials Research Society Symposium Proceedings, vol. 519, MRS, Warrendale, PA, 1998, p. 401.
[7] B. Moraru, G. Kickelbick, U. Schubert, Eur. J. Inorg. Chem. (2001) 1295.
[8] O. Glatter, Acta Phys. Austr. 83 (1977) 47.
[9] O. Glatter, J. Appl. Cryst. 10 (1977) 415.
[10] A. Guinier, G. Fournet, Small-angle Scattering of X-rays, Wiley, New York, 1955.
[11] J.E. Martin, A.J. Hurd, J. Appl. Crystallogr. 20 (1987) 61.
[12] M. Kataoka, J.M. Flanagan, F. Tokunaga, D.M. Engelman, in: B. Chanse, J. Deisenhofer, S. Ebashi, D.T. Googhead (Eds.), Use of X-ray Solution Scattering for Protein Folding Study in Synchrotron Radiation in the Biosciences, vol. 4, Clarendon, Oxford, 1994, pp. 87–92.
[13] O. Glatter, Prog. Colloid Polym. Sci. 84 (1991) 46.
[14] M. Magini, A. Cabrini, J. Appl. Cryst. 5 (1972) 14.
[15] C.J. Pouchert (Ed.), The Aldrich Library of Infrared Spectra, 3rd Ed., Aldrich Chemical Co, WI, USA, 1981.
[16] R.M. Silverstein, F.X. Webster (Eds.), Spectrometric Identification of Organic Compounds, 6th Ed., John Wiley, New York, 1998.
[17] A. Sellinger, P.M. Weiss, A. Nguyen, Y. Lu, R.A. Assink, C.J. Brinker, in: R.M. Laine, C. Sanchez, C.J. Brinker, E. Giannelis (Eds.), Organic/inorganic Hybrid Materials, vol. 519, MRS, USA, 1998, p. 95.
[18] J. Méndez-Vivar, R. Mendoza-Serna, P. Bosch, V.H. Lara, J. Non-Cryst. Solids 248 (1999) 147.
[19] D.C. Bradley, R.C. Mehrotra, D.P. Gaur, Metal Alkoxides, Academic, London, 1978.
[20] C. Sanchez, F. Babonneau, S. Doeuff, A. Leaustic, in: J.F. Mackenzie, D.R. Ulrich (Eds.), Ultrastructure Processing of Advanced Ceramics, Wiley, New York, 1988, p. 77.
[21] J. Méndez-Vivar, C.J. Brinker, J. Sol–Gel Sci. Tech. 2 (1994) 393.
[22] J. Méndez-Vivar, P. Bosch, V.H. Lara, R. Mendoza-Serna, J. Sol–Gel Sci. Tech. 25 (2002) 249.
[23] J. Méndez-Vivar, R. Mendoza-Serna, L. Valdez-Castro, J. Non-Cryst. Solids 288 (2001) 200.
[24] D.W. Schaefer, J.E. Martin, K.D. Keefer, in: N. Bocarra, M. Daoud (Eds.), Physics of Finely Divided Matter, Springer, Berlin, 1985, p. 31.
[25] L. Valdez-Castro, J. Méndez-Vivar, R. Mendoza-Serna, J. Porous Mater. 8 (2001) 303.
[26] J. Méndez-Vivar, P. Bosch, V.H. Lara, R. Mendoza-Serna, J. Porous Mater. 9 (2002) 231.